ESC
European Society
of Cardiology

Chitinase 3 like 1 is a regulator of smooth muscle cell physiology and atherosclerotic lesion stability

Pavlos Tsantilas [1,2,3†], Shen Lao [3,4†], Zhiyuan Wu[3], Anne Eberhard [1,2], Greg Winski [5], Monika Vaerst [1,2], Vivek Nanda[1,2], Ying Wang [1,2], Yoko Kojima[1,2], Jianqin Ye[1,2], Alyssa Flores[1,2], Kai-Uwe Jarr [1,2], Jaroslav Pelisek[3,6], Hans-Henning Eckstein[3,7], Ljubica Matic[8], Ulf Hedin [8], Philip S. Tsao[9,10], Valentina Paloschi [3,7], Lars Maegdefessel [3,5,7,*,†], and Nicholas J. Leeper [1,2†]

[1]Department of Surgery, Division of Vascular Surgery, Stanford University School of Medicine, 300 Pasteur Drive, Alway Bldg., M121 Stanford, CA 94305, USA; [2]Stanford Cardiovascular Institute, Stanford University School of Medicine, 265 Campus Drive Stanford, CA 94305, USA; [3]Department for Vascular and Endovascular Surgery, Klinikum rechts der Isar, Technical University Munich, Ismaningerstr. 22, 81675 Munich, Germany; [4]Department of Thoracic Oncology and Surgery, China State Key Laboratory of Respiratory Disease and National Clinical Research Center for Respiratory Disease, The First Affiliated Hospital of Guangzhou Medical University, 151 Yanjiang Road, Guangzhou 510120, China; [5]Department of Medicine, Karolinska Institute, Stockholm, Solnavägen 1, 171 77 Solna, Sweden; [6]Department for Vascular Surgery, University Hospital Zurich, Rämistrasse 100, 8091 Zurich, Switzerland; [7]German Center for Cardiovascular Research (DZHK), Potsdamer Str. 58, 10785 Berlin, Germany, partner site Munich Heart Alliance; [8]Department of Molecular Medicine and Surgery, Karolinska Institute, Stockholm, Solnavägen 1, 171 77 Solna, Sweden; [9]Department of Medicine, Division of Cardiovascular Medicine, Stanford University School of Medicine, 870 Quarry Road, Stanford, CA 94305, USA; and [10]Veterans Affairs (VA) Health Care System, 3801 Miranda Ave, Palo Alto, CA 94304, USA

|	
Aims	Atherosclerotic cerebrovascular disease underlies the majority of ischaemic strokes and is a major cause of death and disability. While plaque burden is a predictor of adverse outcomes, plaque vulnerability is increasingly recognized as a driver of lesion rupture and risk for clinical events. Defining the molecular regulators of carotid instability could inform the development of new biomarkers and/or translational targets for at-risk individuals.
Methods and results	Using two independent human endarterectomy biobanks, we found that the understudied glycoprotein, chitinase 3 like 1 (*CHI3L1*), is up-regulated in patients with carotid disease compared to healthy controls. Further, *CHI3L1* levels were found to stratify individuals based on symptomatology and histopathological evidence of an unstable fibrous cap. Gain- and loss-of-function studies in cultured human carotid artery smooth muscle cells (SMCs) showed that *CHI3L1* prevents a number of maladaptive changes in that cell type, including phenotype switching towards a synthetic and hyperproliferative state. Using two murine models of carotid remodelling and lesion vulnerability, we found that knockdown of *Chil1* resulted in larger neointimal lesions comprised by de-differentiated SMCs that failed to invest within and stabilize the fibrous cap. Exploratory mechanistic studies identified alterations in potential downstream regulatory genes, including large tumour suppressor kinase 2 (*LATS2*), which mediates macrophage marker and inflammatory cytokine expression on SMCs, and may explain how *CHI3L1* modulates cellular plasticity.
Conclusion	*CHI3L1* is up-regulated in humans with carotid artery disease and appears to be a strong mediator of plaque vulnerability. Mechanistic studies suggest this change may be a context-dependent adaptive response meant to maintain vascular SMCs in a differentiated state and to prevent rupture of the fibrous cap. Part of this effect may be mediated through downstream suppression of *LATS2*. Future studies should determine how these changes occur at the molecular level, and whether this gene can be targeted as a novel translational therapy for subjects at risk of stroke.

* Corresponding author. Tel: +49 89 41403490, E-mail: lars.maegdefessel@tum.de
† These authors contributed equally to the study.

Graphical Abstract
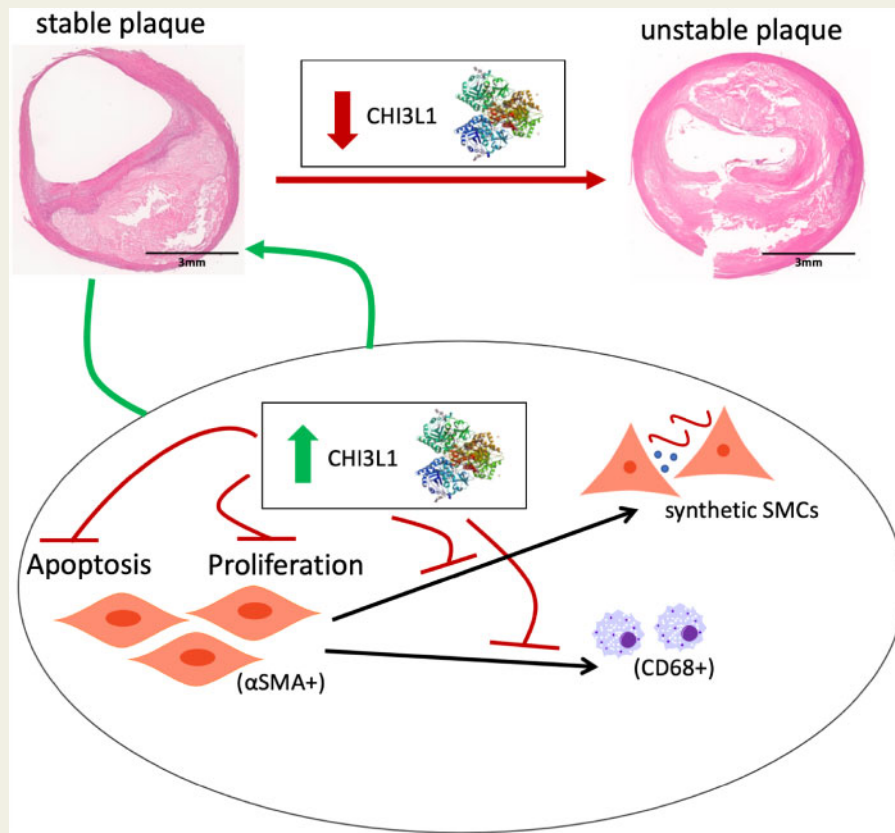
1. Introduction

Atherosclerotic cardiovascular disease (CVD) is the leading cause of morbidity and mortality worldwide.[1,2] Atherosclerotic plaques can accumulate within the coronary, the carotid, or the peripheral vasculature, where they can cause heart attack, stroke, or limb ischaemia, respectively. About half of all strokes are ischaemic in nature (in contrast to haemorrhagic strokes),[2] and typically result from a transient or permanent reduction in cerebral blood flow.[3]

However, it is now recognized that risk of stroke is not solely related to severity of arterial stenosis,[4] which is still the main decision variable for carotid endarterectomy (CEA).[5] Instead, recent data suggest that it is the composition of the plaque, which influences its vulnerability and propensity for rupture. Plaques with a thin fibrous cap, a lipid-rich necrotic core, inflammatory infiltrates, neo-vessel growth, and intra-plaque haemorrhage are considered 'vulnerable'.[4] Several mechanisms have been proposed as potential contributors to these processes, many of which regulate smooth muscle cell (SMC) differentiation, proliferation, and/or apoptosis, and their ultimate contribution to the stabilizing fibrous cap.[6]

Transcriptomic and proteomic profiling studies in symptomatic and asymptomatic patients undergoing CEA at the Karolinska Institute in Stockholm identified chitinase 3 like 1 (human gene: *CHI3l1,* human

protein: CHI3L1, mouse gene: *Chil1*, mouse protein: Chil1,[7] also known as YKL-40, BRP-39, cartilage glycoprotein 1, GP-39, and HcGP-39[8]) as one of the most substantially up-regulated markers in symptomatic patients.[9] CHI3L1 has previously been identified as a reproducible biomarker in several chronic inflammatory diseases (e.g. asthma, rheumatoid arthritis and diabetes-associated vascular diseases, etc.).[10–22] It is further known that CHI3L1 is expressed by various cell types of importance to atherosclerotic CVD, including macrophages, neutrophils, endothelial cells, SMCs, and fibroblasts, and is regulated by a variety of inflammatory cytokines [e.g. interleukin 1 beta (IL1β), IL6, tumour necrosis factor (TNF), and interferon-γ].[8] Work from our own labs have discovered that CHI3L1 mediates vascular inflammation *via* direct regulation of miR-24 in progressing abdominal aortic aneurysms.[23] While elevated CHI3L1 levels have previously been reported in subjects with carotid atherosclerosis,[24] it remains unclear whether these changes are causal or compensatory, given the existence of conflicting mechanistic studies regarding its fundamental role in vascular biology.[10,23,25–29]

In an effort to explore the biology behind increased *CHI3L1* levels, we measured its mRNA expression in laser-captured, micro-dissected fibrous caps harvested from individuals undergoing CEA at the Technical University Munich. Here, *CHI3L1* was found to be significantly increased in unstable vs. stable fibrous caps from advanced lesions. This finding

generated the basis for this study, where the aim was to integrate *in vitro*, *ex vivo*, and *in vivo* models to decipher the role of CHI3L1 in advanced atherosclerosis and plaque vulnerability.

2. Methods

2.1 Analysis of human biobank specimens

2.1.1 Biobank of Karolinska Endarterectomies
The Biobank of Karolinska Endarterectomies (BiKE) from Stockholm, Sweden is a prospective collection of atherosclerotic plaques received after CEA for high-grade carotid artery stenosis. Patient clinical parameters, sample collection and processing, and methods applied in this biobank have been described elsewhere in detail.[9,30] The same definition as elaborated below in the Munich Vascular Biobank was used to differentiate asymptomatic from symptomatic patients. Human studies from BiKE are approved by the Ethical Committee of Stockholm and follow the guidelines of the Declaration of Helsinki. All human samples and data in BiKE are collected with informed consent from patients or organ donors' guardians. For microarrays, non-atherosclerotic iliac arteries and one aorta from healthy individuals (*n*=10) were compared with carotid plaques (*n*=127), where 40 were from asymptomatic and 87 from symptomatic patients at the time of CEA. The full dataset can be accessed from Gene Expression Omnibus with the number GSE21545. For proteomics, CEA tissue specimens from *n*=18 patients matched for male gender, age, and statin medication were analysed using liquid chromatography-mass spectrometry/mass spectrometry (LC-MS/MS), as previously described in detail.[30–32] Further, gene expression correlation studies with the carotid artery plaques were performed.

2.1.2 Munich Vascular Biobank
Plaque specimens from the Munich Vascular Biobank were used to study gene expression in laser-captured, micro-dissected fibrous caps and to perform immunohistochemical analyses, as shown before[33] and described below. The Munich Vascular Biobank contains more than 1700 human atherosclerotic plaques and plasma samples, along with clinical data obtained from patients receiving CEA.[34] Informed written consent was obtained from each patient, and studies follow the guidelines of the Declaration of Helsinki. Age-, gender-, and medication-matched samples from 10 asymptomatic patients with histologically stable plaques were compared with 10 symptomatic patients with histologically unstable plaques. Symptomatic stenosis was defined if the patient had suffered from carotid related symptoms, such as transient ischaemic attack, amaurosis fugax, or stroke, within the last 6 months. Plaque stability was defined as described by Redgrave *et al.*[35] An unstable lesion was defined as a ruptured or rupture-prone plaque with a fibrous cap of <200 μm overlying the necrotic core. Conversely, stable lesions were defined as those having a thick fibrous cap (≥200 μm) or those without a lipid or necrotic core.

2.1.3 Laser capture micro-dissection of advanced atherosclerotic carotid artery plaques
Atherosclerotic lesions were embedded in paraffin, then sectioned, and finally stained with haematoxylin and eosin (H&E) on RNase-free glass slides, using a standardized protocol being described before.[33,36] In brief, RNA extraction from catapulted, micro-dissected samples was performed using the RNeasy Micro Kit (Qiagen, Venlo, the Netherlands) following manufacturer's protocol. RNA was quantified by Nanodrop

(Agilent Technologies, Santa Clara, CA, USA) and RNA quality was verified using an Agilent 2100 Bioanalyzer (Agilent Technologies). The TaqMan High Capacity cDNA Transcription Kit (Thermo Fisher Scientific, Waltham, MA, USA) was used for cDNA synthesis, and primer assays for *CHI3L1*, large tumour suppressor kinase 2 (*LATS2*), and glyceraldehyde 3-phosphate dehydrogenase (*GAPDH*) (all from Thermo Fisher Scientific) and others (see Supplementary material online) were utilized to detect expression changes.

2.1.4 Immunohistochemistry of human carotid plaques
Atherosclerotic plaques were embedded in paraffin, sectioned at 7 μm thickness, and then stained after a standardized protocol (see Supplementary material online, *Table S1* for immunohistochemistry and *Table S2* for immunofluorescence staining). Antibodies used for staining are described in the Supplementary material online, Methods. Images were scanned using the PreciPoint M8 digital microscope system (PreciPoint, Freising, Germany) for immunohistochemistry and FV3000 (Olympus, Hamburg, Germany) for immunofluorescence staining.

2.2 *In vitro*

2.2.1 Primary cell culture
For primary cell culture experiments, we used human carotid artery smooth muscle cells (HCtASMC) from Cell Applications (San Diego, CA, USA). Cells were cultivated in accordance with the manufacturers' instructions in 5% CO_2 atmosphere at 37°C. After reaching 70–80% confluence, cells at passage number 4–6 were used for all further experiments. Cells were treated under different conditions including normal serum, mechanical stress (scratch wound injury), or inflammatory stimuli, such as oxidized low-density lipoprotein (oxLDL, Thermo Fisher Scientific) and lipopolysaccharides (LPSs, Sigma Aldrich, St. Louis, MO, USA). For mechanical stress, a scratch wound injury was performed using the IncuCyte Wound Maker tool (Essen Bioscience, Michigan, USA) and mRNA expression was measured 24 h after injury compared to normal controls. For oxLDL and LPS, cells were serum starved and treated with oxLDL (100 μg/mL) or LPS (10 μg/mL) for 12 or 48 h, respectively.

2.2.2 Gene modulation
For gene overexpression, we used a specific recombinant plasmid DNA (pCMV6-*CHI3L1*) and a pCMV6 empty vector for negative control (OriGene Technologies, Rockville, MD, USA). The plasmid map is shown in the Supplementary material online, *Figure S1A*. After assessing transfection efficiency, a plasmid concentration of 5 ng/μL was used for further experiments (see Supplementary material online, *Figure S1B*). Cell transfection was performed with lipofectamine 3000 transfection kit (Invitrogen, Carlsbad, CA, USA). For *CHI3L1* knockdown, we used a gene-specific 27mer small interfering RNA (siRNA) and a universal scramble control (OriGene Technologies). Three different gene-specific siRNAs were generated (see Supplementary material online, *Table S3*). Transfection was performed with RNAiMAX (Invitrogen). siRNA SR318700A was identified as having the highest knockdown efficiency by quantitative real-time polymerase chain reaction (qRT–PCR, see below). A concentration of 60 pmol was found to be most effective in a dose-dependent study and was used for further experiments (see Supplementary material online, *Figure S1B*). A similar approach was performed to identify the most effective dose of *LATS2* siRNA. In this case, a concentration of 30 pmol was found to be most effective (see Supplementary material online, *Figure S1C*). The effect of *CHI3L1* modulation on protein expression was measured with western blot analysis

(see Supplementary material online, *Figure S1D*). A detailed description of the western blot analysis protocol can be found in the Supplementary material online, *Table S4*.

2.2.3 RNA isolation and qRT–PCR

Cells were harvested at 24 and 48 h after transfection. Isolation of RNA was performed with RNeasy Plus Mini Kit (Qiagen) following the manufacturer's protocol. To generate equivalent amounts of cDNA, RNA concentrations were measured with a Spectrophotometer (NanoDrop 2000 C, Thermo Fisher Scientific). cDNA was synthesized with the High Capacity RNA-to-cDNA Kit (Thermo Fisher Scientific). Reaction took place in the StepOnePlus RT–PCR System (Thermo Fisher Scientific) (see Supplementary material online, *Table S5*). Normalization of quantification was performed with the housekeeping genes ribosomal protein lateral stalk subunit P0 (*RPLP0*) or *GAPDH*.

2.2.4 Live-cell imaging analysis

To assess the effect of *CHI3L1* on proliferation, migration, and apoptosis in cell culture, we used a live-cell imaging analysis system (IncuCyte, Essen Bioscience), in which cells that are cultured in a standard incubator (Thermo GmbH, Langenselbold, Germany) can be analysed. The IncuCyte captures real-time images (phase contrast and fluorescence) from assay microplates. After training and adjusting the device to detect cells correctly, the software performs an application-specific quantitative imaging analysis. IncuCyte Scratch Wound Assay for migration, confluence assay for proliferation, and IncuCyte Apoptosis Assay for apoptosis were used following the procedure-specific protocol and are described in the Supplementary material online, Methods. Images were automatically analysed by the IncuCyte ZOOM software. Per group, three replicates were performed. Data were presented as the mean with standard deviation.

2.2.5 RNA sequencing

RNA sequencing (RNAseq), was performed using the Ion Torrent Ion S5 system (Thermo Fisher Scientific) in HCtASMC using the same overexpression and negative control conditions as described above (*n*=4 per group). Libraries were prepared using the Ion Torrent Ion Total RNA-Seq Kit v2 and Ion Xpress RNA-Seq Barcode 1-16 Kit (Thermo Fisher Scientific). Data analysis was performed using Bioconductor v3.10/RStudio v1.1.463/R v3.5.3. Based on multidimensional scaling (see Supplementary material online, *Figure S2A*), two samples—one in each group, were considered outliers and excluded from further analysis, leaving us with three samples in each group. Mapped gene reads were analysed for differential expression using the edgeR library (v3.24.3). From 55 765 mapped genes, 11 096 remained after performing basic filtering using default edgeR settings—selecting only genes with a count-per-million CPM of at least 10 in each analysed sample. In total, 225 differentially expressed genes were identified (fold-change >1.5 and Benjamini–Hochberg FDR<0.05). To allow a more stringent analysis, Kyoto Encyclopaedia of Genes and Genomes (KEGG) pathway analysis was performed using limma (v3.38.3, see Supplementary material online, *Figure 2B and C*).[37]

2.3 *In vivo*

All animal protocols used were approved by the Stanford University Administrative Panel on Laboratory Animal Care (protocol 27 279). All animal procedures performed conform to the current NIH guidelines. For anaesthetic agent, we used isoflurane 1–3% per inhalation and for analgesics lidocaine 2–4 mg/kg local subcutaneously before surgical incision, bupivacaine 1–2 mg/kg local subcutaneously before surgical incision, and carprofen 5–10 mg/kg pre-operatively subcutaneously. Response of mice to pain stimulation was monitored to assess adequacy of anaesthesia. For this, withdrawal reflex was assessed before incision and after 10 min. Immediately after surgery, mice were monitored every 15 min until full awake and recovered (=righting-reflex has returned, and mice were fully mobile) in a separate cage with flat bedding and half of the cage supplemented with heat. Once recovered, they were returned to their home cage. Mice were monitored postoperatively twice daily for the first three days, then daily for the remaining experiment. If found in pain (irritation, scratching, hunched, or scruffy), carprofen was injected subcutaneously. Rodents were euthanized under full anaesthesia with isoflurane 1–3% and cardiac exsanguination. Cervical dislocation was used as a secondary method of euthanasia.

2.3.1 Carotid ligation and induced plaque rupture in mice

For functional studies, we used two animal surgery models (see Supplementary material online, *Figure S3*). The first was the carotid ligation model (CLM), which was used to induce vascular remodelling.[38] This model helps to investigate the process of vascular intimal proliferation and thus is helpful to measure SMC function and differentiation status. The second surgery model was the inducible plaque rupture model (PRM). This model utilizes a modified version of the carotid ligation/cast approach first described by Sasaki *et al.*,[39] which can be used to measure lesion vulnerability and fibrous cap stability. Both models are described in detail in the Supplementary material online, Methods and *Figure S3*.

2.3.2 Phenotype mouse models

The CLM (see Supplementary material online, *Figure S3*) was performed using common wild-type C57BL/6J mice that were fed standard chow diet (Stock Number: 000664, Jackson Laboratory, Bar Harbour, Maine, USA). For the inducible PRM (see Supplementary material online, *Figure S3*), we used dyslipidaemic *Apoe*^{−/−} mice that were fed a high-fat diet (Stock Number: 002052, Jackson Laboratory). To assess phenotype switching in the inducible PRM, *Myh11*-Cre[ERT,2] Rosa26-Tomato^{+/-}, and *Apoe*^{−/−} SMC lineage-tracing mice (Tomato mice) were provided by Stanford University.

2.3.3 *In vivo* Chil1 inhibition

In vivo knockdown or knockout of the gene of interest was performed with single-stranded antisense oligonucleotides (GapmeRs, Qiagen), which induced RNase H-dependent degradation of complementary RNA targets. Oligonucleotides with unspecific binding sequence ordered from stock from the same company (Qiagen), were used as negative controls at the same dose. Sufficient knockdown of *Chil1* with GapmeRs was tested *in vitro* and in a small pilot study of four mice (see Supplementary material online, *Figure S4*). More experimental details are provided in the Supplementary material online.

2.3.4 Tissue processing, histology, and immunohistochemistry

Tissue samples were formalin-fixed and then embedded in OCT after sucrose-dehydration. Beginning at the suture, consecutive 7 μm thin sections of the carotid were then cut caudally to the suture until the intimal proliferation or plaque was no longer visible. Sections were marked according to their distance from the suture. Selected sections were then stained with H&E and other immunohistochemical probes as follows: in

the CLM, all morphologic measurements and lesion areas were calculated at distances 200, 400, 600, and 800 μm proximal to the suture, then averaged. For immunohistochemistry sections, samples were analysed 400 μm from the suture. In the PRM, the most advanced lesion upstream of the suture and downstream of the cuff were selected for staining. Samples of the CLM were excluded if there was a lumen at the suture area or if there was no lesion formation, indicating failure of the surgical procedure. Samples of the PRM were excluded if there was no lesion formation, complete thrombosis in the absence of an advanced plaque, or complete luminal occlusion due to intimal proliferation, similar to methods described by Hartwig *et al.*[40] The fibrous cap was defined as the 20 μm of the plaque nearest to the vessel lumen. H&E staining was performed by a standard protocol (Supplementary material online, *Table S6*). Primary and secondary antibodies used are described in the Supplementary material online, Methods. Immunohistochemistry was performed using a standard protocol (see Supplementary material online, *Table S7*). For detection of *in vivo* proliferation, we used an EdU (5-ethynyl-2'-deoxyuridine) proliferation assay: intraperitoneal injection of 50 mg/kg EdU (A10044, Thermo Fisher Scientific) was performed in all mice 24 h before sacrifice. For staining, Click-iT™ EdU Alexa Fluor™ 647 HCS Assay (C10356, Thermo Fisher Scientific) was used according to the manufacturer's instructions. To detect cell apoptosis both conventional cleaved caspase-3 staining and staining for DNA strand breaks (Terminal deoxynucleotidyl transferase dUTP nick end labelling, TUNEL) using the *In Situ* Cell Death Detection Kit, Fluorescein (Sigma, Cat# 11684795910) was performed according to the manufacturer's instructions.

2.4 Image analysis and statistics

Image analysis of *in vivo* experiments was performed with FIJI (ImageJ Version 2.0). Vessel area was calculated with the lasso tool in mm^2. Total vessel area was defined as the region containing the media, intima, and lumen. The medial area was defined by subtracting the intimal and luminal areas from the total vessel area. The intimal area was defined as the intima subtracted by the luminal area. For quantitative immunohistochemistry analyses, each stain was identified using a Region of Interest (ROI) analysis. For example, the fibrous cap was defined with the lasso tool and the 'make band' tool in FIJI, and the ROI was quantified as the circumferential area within 20 μm of the lumen. The individual channels of each immunohistochemistry image were converted into 8-bit greyscale images with a range of 0= black to 255= white. Within this range, a threshold cut point was defined. This threshold cut point allowed distinction of pixels stained by the specific antibody (above threshold; positive) or not stained (below threshold; negative). The ratio of above threshold area/total area was used to define the 'percentage antibody-positive area'. For each antibody, the same threshold was used, and pictures were captured under identical camera settings. For calculation of proliferation and apoptotic index, the channel for cell core and EdU+/TUNEL+ was converted into a binary picture, respectively. The number of cell cores and EdU+/TUNEL+ cells were calculated with the 'Analyse Particles' tool. The index was calculated by EdU+/all cell cores = proliferation-index and TUNEL+/all cell cores = apoptotic index within the different ROIs. For *in vitro* cell culture and *in vivo* experiments, statistical analysis was performed in GraphPad Prism 7 or 8 (GraphPad Software Inc., San Diego, USA). First, normality of distribution was assessed by using D'Agostino and Pearson omnibus tests. Homogeneity of variance was tested with F-test or Levene's test. Normally distributed data were analysed with two-sided Student's *t*-test. Otherwise, non-parametric Mann–Whitney *U* testing was performed. For analysis of multiple gene expression panels, *t*-tests corrected for multiple comparisons using the Holm–Sidak method was performed. For the IncuCyte experiments, both *t*-tests corrected for multiple comparisons using the Holm–Sidak method for each individual time point and two-way repeated measures ANOVA for the entire time course were performed. Differences of RNA level expression were calculated using the $^{\triangle\triangle}$Ct method. Microarray and LC-MS/MS dataset analyses in BiKE were performed with the GraphPad Prism 6 and Bioconductor software, using a linear regression model adjusted for age and gender to check for any association with covariates, and a two-sided Student's *t*-test assuming non-equal deviation to compare groups. *P*-value <0.05 was considered as statistically significant.

3. Results

3.1 *Chi3l1* is increased in patients with symptomatic carotid artery disease and unstable fibrous caps

High transcript expression levels of *CHI3L1* were initially discovered in patients with advanced carotid artery disease in the BiKE cohort. Compared to non-atherosclerotic artery controls, *CHI3L1* was found to be significantly up-regulated in plaques (fold-change 33.2, *P*=0.0001). Moreover, *CHI3L1* was significantly higher expressed in lesions from individuals with symptomatic vs. asymptomatic disease (fold-change 1.6, *P*<0.0001; *Figure 1A*). Further, *CHI3L1* was also up-regulated in plaque specimens from patients with preoperative cardiovascular events vs. those that have not previously suffered an adverse clinical event (fold-change 1.5, *P*=0.04; *Figure 1A*). In addition to changes in mRNA expression, CHI3L1 protein levels were also confirmed to be higher in plaques compared to matched adjacent non-diseased arterial control tissues (fold-change 1.2, *P*=0.0005), and in plaques from symptomatic patients compared to asymptomatic ones (fold-change 1.4, *P*=0.0001; *Figure 1B*).

In addition to the changes in *CHI3L1* in bulk plaque tissue, we measured its expression in laser-captured, micro-dissected fibrous caps from unstable/ruptured plaques vs. stable plaques (*n* = 10 each). Here, *CHI3L1* was significantly increased in ruptured compared to stable fibrous caps (fold-change 2.1, *P*=0.0089; *Figure 1C*). To further investigate the localization of CHI3L1 during lesion formation, we also performed immunofluorescent and immunohistochemical stains of stable and unstable atherosclerotic human carotid plaques. CHI3L1 was predominantly expressed on those lesional SMCs which still expressed SMC differentiation markers [alpha smooth muscle actin (αSMA)] in advanced unstable plaques (*Figure 1D*, see Supplementary material online, *Figure S5*). This finding contrasts with results from stable plaques, where overall CHI3L1 expression was low, and co-localization with SMC markers was minimal (*Figure 1D*, see Supplementary material online, *Figure S5*).

To further investigate the association of *CHI3L1* with genes implicated in inflammation and SMC differentiation, we performed gene expression correlation studies on CEAs from the BiKE cohort. We found that *CHI3L1* mRNA levels were indeed positively correlated with features of plaque vulnerability, such as inflammatory cytokines (e.g. *TNF*; *IL1β*; chemokine ligand 2 (*CCL2*); and *CCL5*), macrophage markers (e.g. cluster of differentiation family: *CD40, CD11a, CD11b, CD11c, CD163, CD274*; fatty acid binding protein 4), and apoptosis markers (e.g. Caspase 3), and inversely-correlated with markers of lesion stability [including the established SMC differentiation markers αSMA/actin alpha 2 (*ACTA2*); myosin-
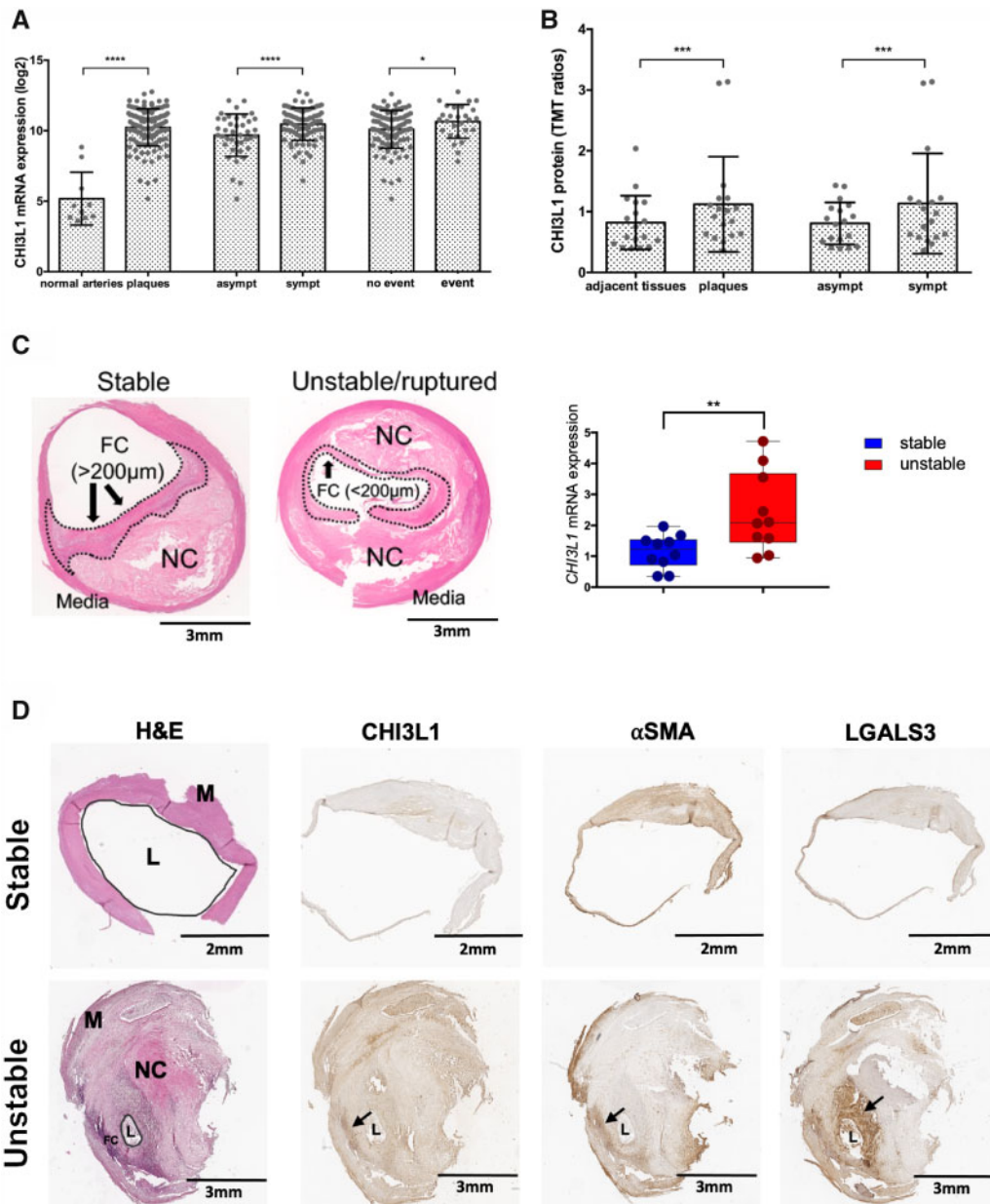
Figure 1 CHI3L1 mRNA and protein expression in human plaques. (*A*) BiKE mRNA expression analysis of *CHI3L1* by microarrays. Normal arteries: *n* =10 (iliac and one aorta), carotid plaques: *n*=127, asympt: *n*=40 plaques from patients asymptomatic at surgery, sympt: *n*=87 plaques from patients symptomatic at surgery, event: indicates previous cardio- or cerebrovascular event *n*=27, no event *n*=98. *CHI3L1* mRNA expression fold-change: plaques vs. normal =+33.2, *P*<0.0001, sympt vs. asympt =+1.6, *P*<0.0001, yes vs. no =+1.5, *P*=0.04. Statistical test: linear regression model and Student's *t*-test. (*B*) BiKE protein quantification of CHI3L1 by LC-MS. Adjacent tissues: *n*=18 matched adjacent arterial tissues used as controls, plaques: *n*=18 carotid plaques, asympt: *n*=18 plaques from patients asymptomatic at surgery, sympt: *n*=18 plaques from patients symptomatic at surgery. CHI3L1 protein fold-change: plaques vs. adjacent =+1.23, *P*=0.0005, sympt vs. asympt =+1.38, *P*=0.0001. Statistical test: see (*A*). (*C*) *CHI3L1* mRNA expression of laser capture micro-dissection of human fibrous cap of 10 stable plaques vs. 10 unstable plaques of the Munich Vascular Biobank. Scale bar: 3 mm. *CHI3L1* expression fold-change: +2.1, *P*=0.0089. Shown as mean±SEM. Statistical test: Student's *t*-test. (*D*) H&E and immunohistochemistry of human atherosclerotic plaques from the Munich Vascular Biobank. CHI3L1 and αSMA co-stain in advanced unstable plaques. Stable plaques show low CHI3L1 expression and minimal co-localization with αSMA. Scale bar: 2 mm (stable), 3 mm (unstable). **P*<0.05; ***P*<0.01; ****P*<0.001, *****P*<0.0001; n.s., non-significant; TMT, tandem mass tag; M, media; NC, necrotic core; FC, fibrous cap; H&E, haematoxylin and eosin stain; CHI3L1, chitinase 3 like 1; αSMA, alpha smooth muscle actin; LGALS3, galectin-3.

11 (*MYH11*); myocardin; smoothelin; and transgelin)] (see Supplementary material online, *Figure S6*).

3.2 Chi3l1-mediated effects on SMC migration, proliferation, and apoptosis

Based on our findings from profiling high-risk carotid artery lesions and the suggested co-localization of CHI3L1 with αSMA-positive cells, we investigated phenotypic and functional changes in disease-relevant HCtASMCs upon *CHI3L1* modulation (*Figure 2A–E*). Interestingly, siRNA-based knockdown of *CHI3L1* significantly increased proliferation compared to (scramble-transfected) controls when using the IncuCyte dynamic live-cell imaging system (*P*=0.0021, *Figure 2A*). Plasmid-based overexpression of *CHI3L1* had opposing results and led to a decrease in proliferation rates over time (*P*<0.0059, *Figure 2A*). Further, *CHI3L1* knockdown led to an increase in SMC apoptosis (*P*<0.0001, *Figure 2B*). Here, *CHI3L1* overexpression did not affect SMC survival compared to the control group (*Figure 2B*). Finally, we used the IncuCyte scratch wound assay to determine the effect of *CHI3L1* modulation on SMC migration. Neither inhibition nor overexpression of *CHI3L1* led to significant differences in the migratory response (*Figure 2C*).

3.3 *Chi3l1* is induced by pro-inflammatory stimuli in SMCs and triggers their trans-differentiation

To assess whether *CHI3L1* modulation is involved in phenotypic and pro-inflammatory changes in HCtASMCs, we investigated the expression of *ACTA2* and cluster of differentiation 68 (*CD68*) upon *CHI3L1* inhibition and overexpression. Interestingly, *CHI3L1* knockdown significantly increased *CD68*-expression (*P*=0.0335, *Figure 2D*), while *CHI3L1* overexpression was not associated with a significant change in *CD68* mRNA levels (*Figure 2D*). Knockdown of *CHI3L1* further resulted in a significant reduction of *ACTA2*-expression (*P*=0.0455, *Figure 2D*), while *CHI3L1* overexpression was not associated with a significant change in *ACTA2* mRNA levels (*Figure 2D*). We further found that HCtASMCs exposed to the pro-atherogenic inflammatory stimulus oxLDL down-regulate classic SMC differentiation markers and up-regulate macrophage markers, such as *LGALS3* (see Supplementary material online, *Figure S7A*). Knockdown of *CHI3L1* under oxLDL conditions exacerbated these findings, leading to additional down-regulation of *ACTA2* and up-regulation of macrophage (*LGALS3*) and inflammatory markers (*IL6, IL1β*) (*Figure 2E*). *CHI3L1* was also suppressed under oxLDL conditions, while other stimuli like toxic inflammatory LPS or mechanical stimuli (scratch wound injury) had no effect (see Supplementary material online, *Figure S7A–C*).

3.4 Role of *Chi3l1* in murine models of vascular remodelling and plaque rupture

To address the impact of *Chi3l1* on vascular remodelling and intimal proliferation, we performed H&E staining at standardized distances proximal to the suture in mice subjected to carotid artery ligation. A variety of endpoints, including total area, vessel area, medial area, intimal area, and luminal area were assessed upon H&E staining. The total area of the vessel was significantly larger in the *Chi3l1* GapmeR group compared to scrambled controls (*P*=0.007, see Supplementary material online, *Figure S8A*). The luminal area (*P*=0.012), the vessel area (total area without the lumen, *P*=0.017), and its individual components including the media (*P*=0.017), and intima (*P*= 0.023) were all significantly larger as well (*Figure 3A*, see Supplementary material online, *Figure S8A*). To address the effect on αSMA positive cells, representing the content of differentiated SMCs, we analysed the percentage of αSMA-positive area in the total area, medial area, and intimal area upon carotid ligation. In the *Chi3l1* GapmeR group, the percentage of αSMA positive cells was significantly reduced (*P*=0.016, see Supplementary material online, *Figure S8B*). This effect was not significant when analysing the medial part only (*P*=0.16, see Supplementary material online, *Figure S8B*), but significant in the intimal area alone (*P*=0.007, *Figure 3B*). CD107b (Mac-3), representing macrophages, was expressed equally in both, the *Chi3l1* GapmeR and control groups (see Supplementary material online, *Figure S8C*). In the GapmeR group, the proliferation-index of the vessel was significantly increased compared to the control group (*P*=0.042, *Figure 3C*). No significant differences between both groups regarding the apoptotic index could be measured (*P*=0.244, *Figure 3D*).

Next, we performed the inducible PRM in *Apoe*$^{-/-}$ mice. Immunohistochemistry using antibodies against αSMA and MAC3 revealed no significant differences between groups (see Supplementary material online, *Figure S8D*). Of the analysed arteries, 86% (*n*=6/7) in the control group and 63% (*n*=5/8) in the knockdown group developed an advanced lesion with increased intimal thickening and partial necrotic core formation. To determine the SMC content in fibrous caps, we measured αSMA positive cells in this specific region of the developed plaques. In this area, αSMA positive cells were significantly reduced in the GapmeR group compared to controls (*P*=0.0148, *Figure 4A*). Ter-119 positive cell areas, which indicate erythrocytes inside the intima, were utilized to define intra-plaque haemorrhages. Intra-plaque haemorrhages were present in five of seven mice in the control group (71%), and in six of eight mice in the GapmeR group (75%), showing no statistically significant changes. However, a cross-linked fibrin antibody stain to detect atherothrombotic events in this particular model[33,36] indicated more plaque ruptures in the GapmeR group when compared to controls (*Figure 4B*).

To assess differences in cell-specific phenotype modulation, we performed a small subset study using the Tomato mice system as described above in a total of eight mice. Double immunofluorescent imaging (red fluorescence = initial MYH11 cells, green fluorescence = αSMA positive cells) supported the notion of reduced αSMA expression in SMC-derived cells as a result of *Chi3l1* inhibition (dominant red-coloured plaque in the GapmeR group, *Figure 4C*).

3.5 Potential mediators of *CHI3L1* deregulation in atherosclerosis

Finally, we sought to identify interaction partners and downstream mediators of *CHI3L1* in the context of advanced atherosclerosis. To mimic the elevated levels of *CHI3L1* expression in SMCs in atherosclerosis, we performed RNAseq in HCtASMCs treated with a *CHI3L1* overexpressing plasmid analogous to our cell culture experiments described above. KEGG Pathway over-representation analysis revealed 85 significantly (*P*<0.05) enriched pathways, of which 12 we deemed relevant for disease and tissue phenotype (*Figure 5A*). In the case of the top 10 pathways, we observed significant enrichment of down-regulated genes in each pathway. In the case of the two pathways on the bottom of the panel, we observed significant enrichment of down-regulated genes but also of up-regulated genes in those pathways (*Figure 5A*, see Supplementary material online, *Figure S2B and C*). In order to improve disease-relevance of the final set of differentially expressed genes, we chose to filter out genes within the remaining 73 significantly enriched pathways from further analysis. Following this approach, remaining were 33 genes significantly different between the treatment (*CHI3L1* overexpression) and the
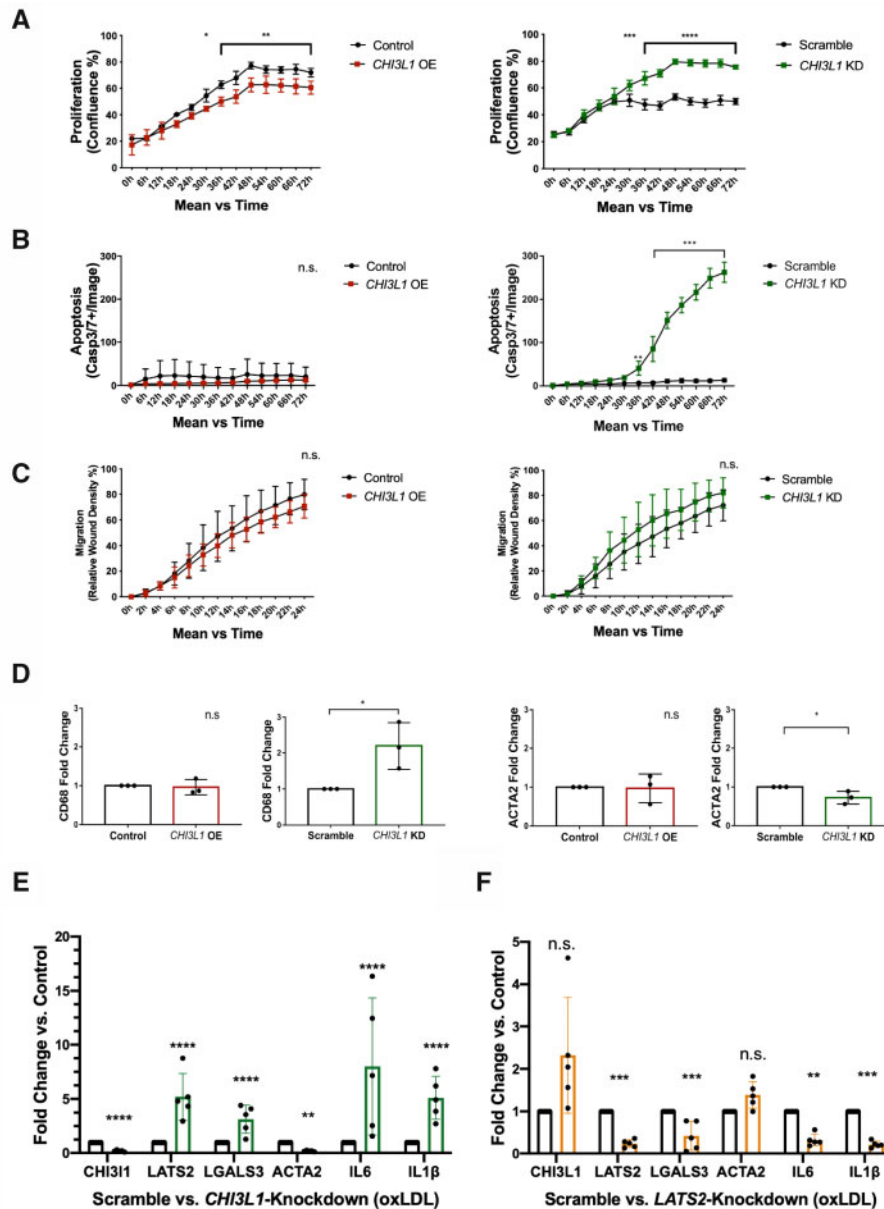
Figure 2 Live-cell imaging analysis to determine the functional role of *CHI3L1* and expression of vascular SMC and macrophage markers upon *CHI3L1* and *LATS2* modulation. Results are presented as the mean±standard deviation. Statistical test IncuCyte: multiple *t*-tests corrected for multiple comparisons (Holm–Sidak) for each individual time point and two-way repeated measures ANOVA for the whole time course. (*A*) Proliferation: occupied area (confluence %, *n*=3), *CHI3L1*-knockdown: *P*=0.0021; *CHI3L1*-overexpression: *P*=0.0059. (*B*) Apoptosis: IncuCyte apoptosis assay (*n*=3). *CHI3L1*-knockdown: *P*<0.0001; *CHI3L1*-overexpression: *P*=0.4210. (*C*) Migration: IncuCyte scratch wound assay (*n*=3). *CHI3L1*-knockdown: *P*=0.1978; *CHI3L1*-overexpression: *P*=0.2526. (*D*) Measurements of relative mRNA levels of the macrophage biomarker (CD68) and vascular SMC biomarker ACTA2 (αSMA). Differences between groups were presented as fold-change with error bars as standard deviation (*n*=3). Statistical test: Student's *t*-test. Knockdown of *CHI3L1*: *CD68* expression (fold-change 2.2, *P*=0.0335), *ACTA2* expression (fold-change 0.7, *P*=0.0455). (*E*) Treatment of HCtASMC with anti-*CHI3L1* siRNA before 12 h of oxLDL (100 μg/mL) exposure (*n*=5). Quantification of mRNA expression with qPCR: *CHI3L1* fold-change 0.2, *P*<0.0001; *LATS2* fold-change 4.9, *P*=0.0002; *LGALS3* fold-change 2.9, *P*=0.006; *ACTA2* fold-change 0.2, *P*=0.0007; *IL6* fold-change 5.7, *P* <0.0001; *IL1β*, fold-change 4.8, *P*=0.0002. Statistical test: Multiple *t*-tests corrected for multiple comparisons using the Holm–Sidak method. (*F*) Treatment of HCtASMC with anti-*LATS2* siRNA before 12 h of oxLDL (100 μg/mL) exposure (*n*=5). Quantification of mRNA expression with qPCR: *CHI3L1* fold-change 1.2, *P*=0.1; *LATS2* fold-change 0.2, *P*=0.001; *LGALS3* fold-change 0.3, *P*=0.004; *ACTA2* fold-change 1.4, *P*=0.4; *IL6* fold-change 0.3, *P*=0.007; *IL1β*, fold-change 0.2, *P*=0.001. Statistical test: Multiple *t*-tests corrected for multiple comparisons using the Holm–Sidak method. **P*<0.05; ***P*<0.01; ****P*<0.001; *****P*<0.0001. n.s., non-significant; OE, overexpression of *CHI3L1*; KD, knockdown of *CHI3L1*; Cas3/7, Caspase 3/7; CD68, cluster of differentiation 68; ACTA2, actin alpha 2; CHI3L1, chitinase 3 like 1, HCtASMC, human carotid artery SMCs; LATS2, large tumour suppressor kinase 2; LGALS3, galectin-3; IL6, interleukin 6; IL1β, interleukin 1 beta; oxLDL, oxidized low-density lipoprotein.

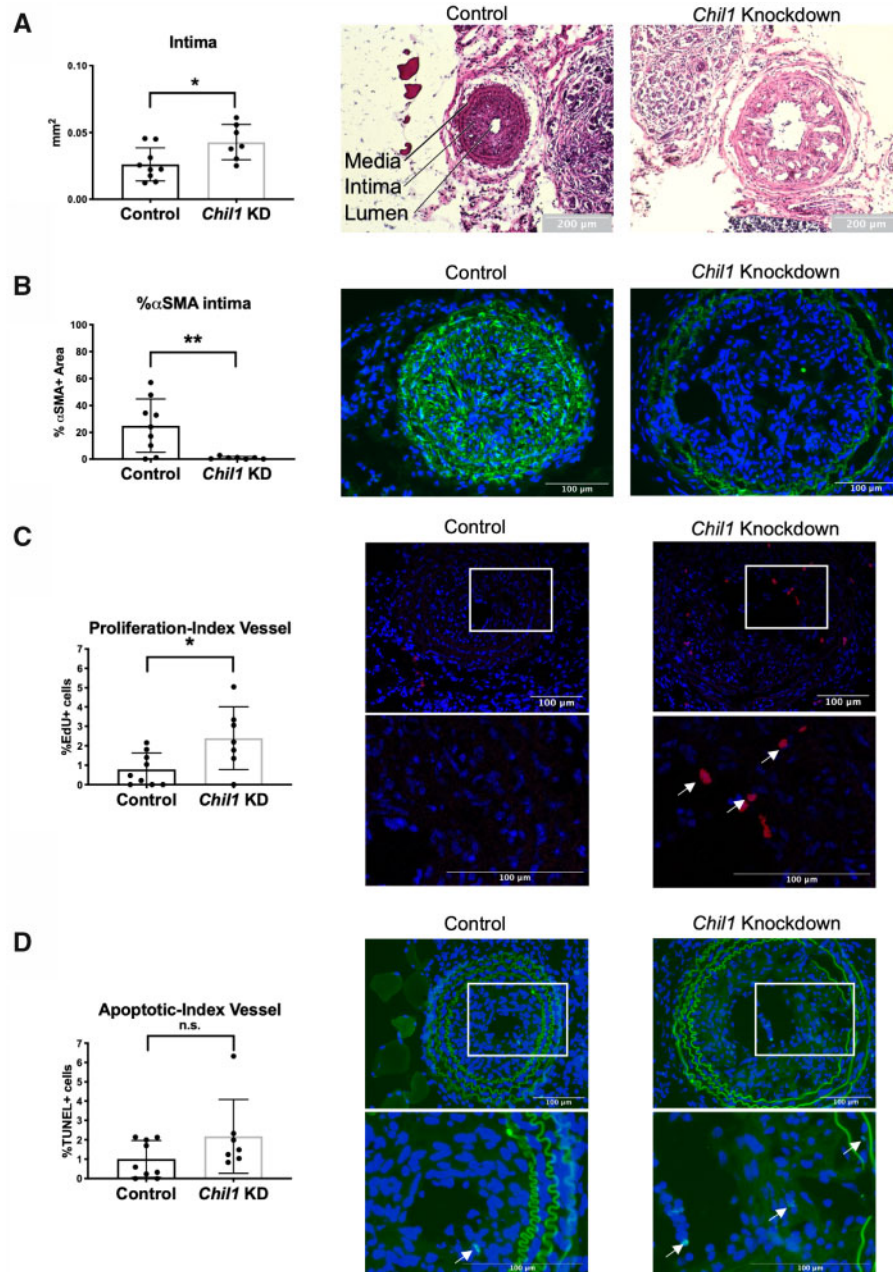**Figure 3** Functional role of *Chil1* in vascular remodelling in the murine CLM. (*A*) Area intima was significantly increased in the knockdown group (*P*=0.0238). Scale bar: 200 μm. (*B*) Measurement of αSMA positive area. Threshold area is divided through the total ROI area and described as '% αSMA+ area'. Knockdown of *Chil1* significantly decreased amount of αSMA staining in intima (*P*=0.0067). Scale bar: 100 μm. (*C*) Proliferation-index in the knockdown group was significantly increased (*P*=0.0419). Scale bar: 100 μm. (*D*) Apoptotic index: non-significant (*P*=0.244). Scale bar: 100 μm. Statistical test for (*A–D*): Student's *t*-test. N=9 vs. 7 mice were used for all experiments (*A–D*). **P*<0.05; ***P*<0.01; ****P*<0.001; n.s., non-significant; αSMA, alpha smooth muscle actin; EdU, 5-ethynyl-2'-deoxyuridine; TUNEL, TdT-mediated dUTP-biotin nick end labelling; Chil1, chitinase 3 like 1.

control group (*Figure 5B*). We identified the six genes being most significantly down-regulated in response to *CHI3L1* overexpression (*Figure 5B*), and further analysed these in HCtASMCs in which *CHI3L1* was inhibited using siRNA (again analogous to our cell culture experiments described above). Interestingly, two out of these six genes [*LATS2* and homeodomain-interacting protein kinase 2 (*HIPK2*)] were

significantly increased upon *CHI3L1* inhibition (*Figure 5C*), suggesting a direct correlation and interaction with *CHI3L1* expression levels in SMCs. When analysing mRNA expression of these two genes in our fibrous caps from ruptured/unstable vs. stable lesions, only the tumour suppressor *LATS2* was significantly deregulated. In accordance with our RNAseq profiling data, where *LATS2* expression was decreased upon high
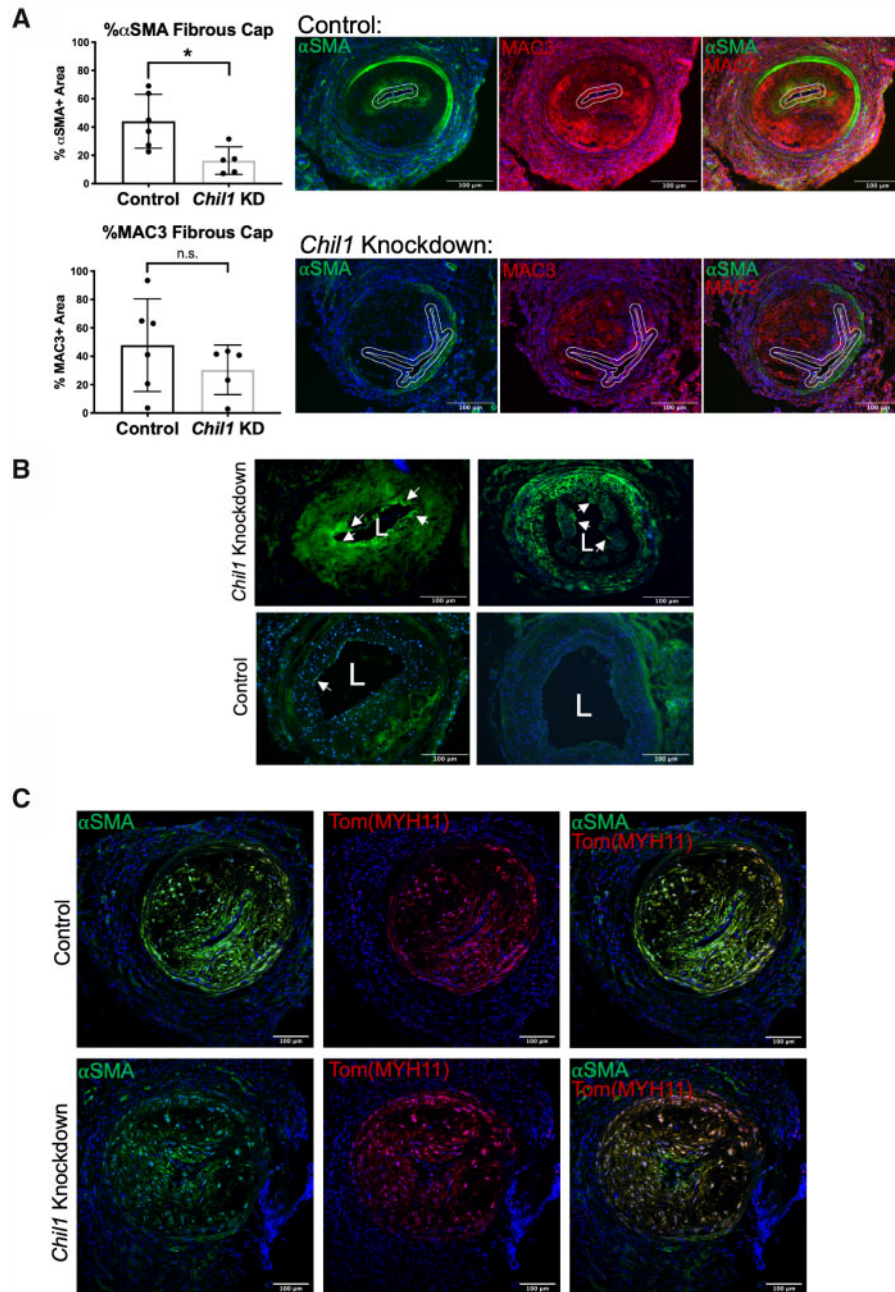
Figure 4 Functional role of *Chil1* on plaque vulnerability in the murine PRM. (*A*) Threshold area is divided through the total ROI area and described as '%+area'. Percentage of αSMA-positive area was significantly reduced in *Chil1* knockdown group (*P*=0.015). No effect was detected when looking at percentage of MAC3-positive area (*P*=0.29). *N*=6 vs. 5 mice. Statistical test: Student's *t*-test. Scale bar: 100 μm. (*B*) Representative picture of images stained with cross-linked fibrin to indicate atherothrombotic events and unstable/ruptured plaques in the inducible PRM in *Apoe*$^{-/-}$. White arrows indicate increased fibrin signal mainly in the Anti-Chil1 group. (*A* and *B*): *N*=6 vs. 5 mice. Scale bar: 100 μm. (*C*) PRM of Tomato mice. Double immunofluorescent imaging (red fluorescence = initial MYH11 cells, green fluorescence = αSMA positive cells) supports results of reduced αSMA expression through down-regulation of Chil1 (red-dominant plaque in the knockdown group). Scale bar: 100 μm. *N*=2 vs. 2 mice. **P*<0.05; ***P*<0.01; ****P*<0.001; n.s., non-significant; αSMA, alpha smooth muscle actin; MAC3, macrophage antigen 3; MYH11, myosin heavy chain 11; Chil1, chitinase 3 like 1.

exposure of *CHI3L1* (overexpression), a similar result (down-regulation of *LATS2* in ruptured/unstable) could be observed in the laser-captured fibrous caps (*Figure 5D*). To further pursue the mechanistic link between *CHI3L1* and *LATS2*, we performed *in vitro LATS2* knockdown studies in cultured HCtASMCs. *LATS2* knockdown suppressed the expression of macrophage markers (*LGALS3*) and inflammatory cytokines (*IL6* and *IL1β*), but had no effect on the SMC differentiation marker, *ACTA2* (*Figure 2F*). Further, *LATS2* was up-regulated in response to the atherosclerotic stimulus oxLDL in cultured HCtASMCs (see Supplementary material online, *Figure S7A*).
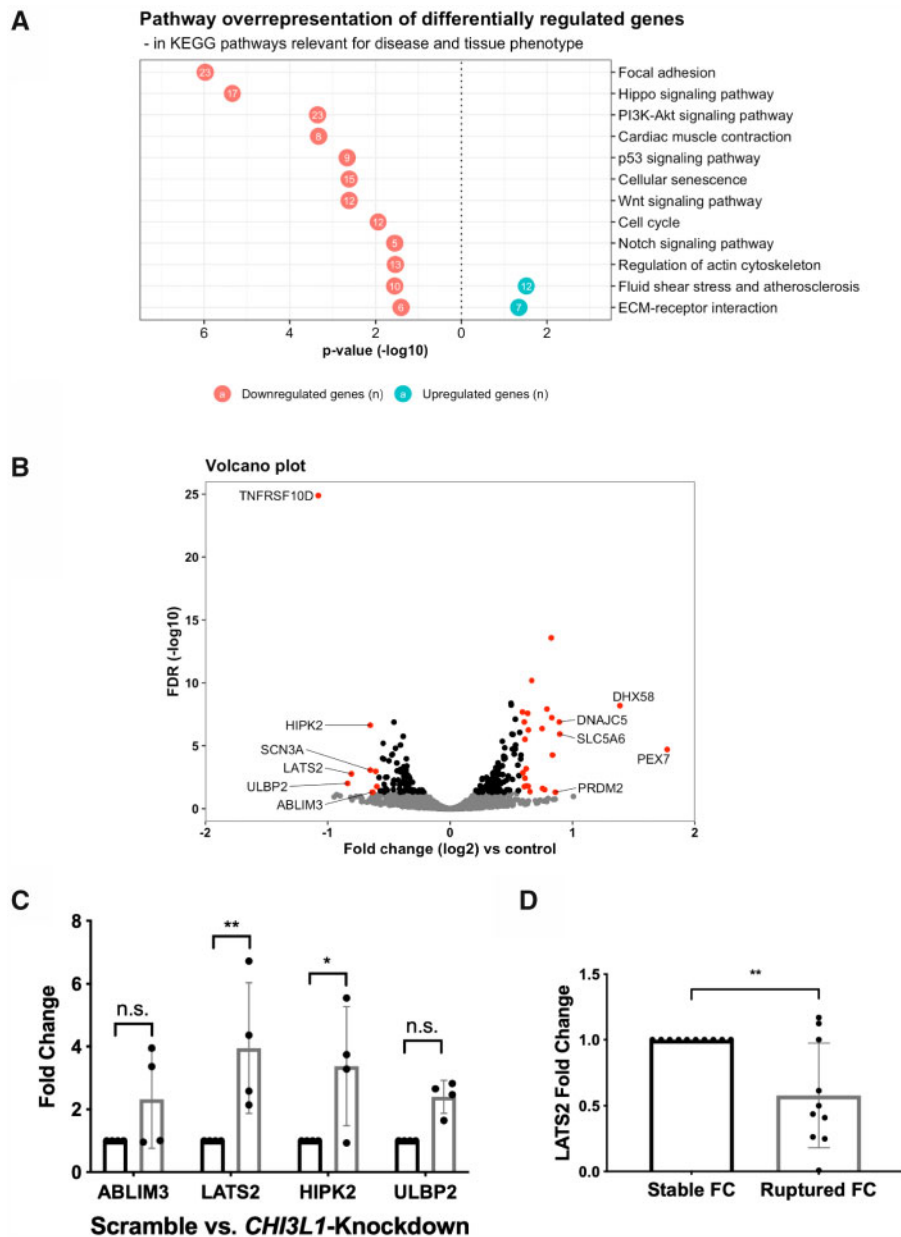
Figure 5 RNAseq to detect downstream effects of *CHI3L1* in human carotid artery SMCs. (*A*) KEGG pathway analysis revealed 12 significantly differentially regulated pathways relevant for disease and tissue phenotype. This approach identifies genes belonging to a given pathway that are significantly up- or down-regulated after CHI3L1 overexpression. Numbers in circles represent the number of genes in the specific pathway that are down-regulated (orange circle) or up-regulated (turquoise circle). (*B*) A total of 33 genes (red dots) were identified as being significantly different between groups (fold-change >1.5 and Benjamini–Hochberg FDR<0.05). The six most significantly down-regulated genes upon *CHI3L1* overexpression were chosen for further analysis. (*C*) All six genes were analysed in HCtASMCs in response to *CHI3L1* knockdown using siRNA (*n*=4 vs. 4). Two genes (*LATS2, P*=0.005; *HIPK2, P*=0.022; *ABLIM3, P*= 0.190; *ULBP2, P*=0.190) were significantly increased upon *CHI3L1* inhibition. Statistical test: multiple *t*-tests corrected for multiple comparisons using the Holm–Sidak method. (*D*) mRNA expression of the two genes being deregulated upon CHI3L1 modulation (inhibition and overexpression) in human fibrous caps from unstable vs. stable lesions (*n*=10 vs. 10). Here, only *LATS2* appeared significantly regulated (*P*=0.0082). Statistical test: Student's *t*-test. *P<0.05; **P<0.01; ***P<0.001; n.s., non-significant; ABLIM3, actin-binding LIM protein 3; LATS2, large tumour suppressor kinase 2; HIPK2, homeodomain-interacting protein kinase 2; ULBP2, UL16 binding protein; SCN3A, sodium channel, voltage-gated, type III, alpha subunit; CHI3L1, chitinase 3 like 1; TNFRSF10D, tumour necrosis factor receptor superfamily member 10D; FC, fibrous cap; SC, scramble; KD, knockdown; FDR, false discovery rate.

4. Discussion

Results from our study indicate that CHI3L1 may not only be a powerful biomarker that can predict the presence of unstable carotid disease, as shown previously[24] but also serve as a key regulator of SMC physiology and thus plaque instability. Specifically, *in vitro* data from human carotid artery SMCs as well as *in vivo* data from two mouse models suggest that *Chil1* prevents SMC 'de-differentiation' and neointimal proliferation, and therefore could represent a novel translational target for the prevention of fibrous cap thinning and atherosclerotic plaque destabilization. Gene expression correlation studies indicate that *CHI3L1* is not only up-regulated in more vulnerable plaques but also shows a clear association with markers of lesional inflammation and loss of stabilizing differentiated SMC content. When considered in the context of our *in vitro* and *in vivo* loss-of function studies, these results suggest that *CHI3L1* up-regulation under pro-atherogenic conditions in the atherosclerotic plaque may represent a compensatory response meant to prevent SMC 'de-differentiation' and inflammation.

CHI3L1 has previously been shown to be elevated in patients with ischaemic CVD[41,42] and advanced atherogenesis in particular.[43] However, this particular biomarker is interesting in that it appears to be differentially expressed under distinct clinical conditions, and perhaps in a tissue- and even vascular bed-specific manner. For example, elevated plasma CHI3L1 levels have been shown to predict the development of ischaemic stroke, but not myocardial infarction.[44,45] While some epidemiological studies have identified an association between YKL-40 and triglyceride levels,[42,46] Mendelian randomization studies have not shown a causal relationship with cholesterol.[46] Instead, YKL-40, which is an acute phase reactant generated by inflammatory cells commonly found in rupture-prone carotid lesions, may be specifically up-regulated in response to the erosion and apoptotic cell death that commonly precedes ischaemic stroke.[47,48]

The mechanism by which CHI3L1 might promote beneficial, plaque stabilizing changes are not yet clear and remains the topic of significant debate. Prior reports indicate that CHI3L1 may dampen the deleterious effects of a wide range of inflammatory cytokines on endothelial cells,[49] myocytes,[50] and fibroblasts.[51] However, CHI3L1 has also been reported to have pro-proliferative effects on SMCs *in vitro*[10,25,29] and atherogenesis *in vivo*.[25–27] The reasons for these diverging results remain unclear but could be related to context-dependent feedback mechanisms that vary according to the presence of upstream inflammatory stimuli or other environmental cues. For example, treatment of isolated HCtASMCs with the pro-atherogenic stimulus oxLDL led to the down-regulation of *CHI3L1 in vitro* (see Supplementary material online, *Figure S7A*), while non-atherogenic stimuli had no effect (see Supplementary material online, *Figure S7B* and *C*), and an inverted pattern was observed in end-stage human carotid plaques (*Figure 1A–C*). The state of disease (early atherogenesis vs. destabilization of existing plaques) appears to be of great importance.

In this study, we find that *CHI3L1* maintains SMCs in a quiescent, differentiated, and non-proliferative state. It also prevents SMC apoptosis and phenotype switching towards a 'macrophage-like' state, *in vitro*. *In vivo*, these properties appear to synergize to prevent SMC 'de-differentiation' and maladaptive vascular changes under both atherosclerotic and non-atherosclerotic conditions. For example, *Chil1* prevented mature SMCs from down-regulating their 'SMC-specific' markers and contributing to the hyperplastic neointima in a carotid injury model, while preserving the number of fully differentiated SMCs in the fibrous cap of lesions from an atherosclerotic carotid PRM. From a molecular mechanism perspective,

hypothesis-free RNAseq studies identified a significant decrease in *LATS2* in cells with high levels of *CHI3L1*. *LATS2* has been previously linked to cancer-related de-differentiation pathways.[52] Being a tumour suppressor gene, *LATS2* might play a significant role in SMC proliferation and differentiation in fibrous cap stability and thus atherosclerotic plaque vulnerability. Results from our *in vitro CHI3L1* and *LATS2* knockdown studies suggest that the beneficial effects of *CHI3L1* up-regulation (inhibition of SMC 'de-differentiation' and inflammation, as shown in *Figure 2D* and *E*) may be dependent on the downstream suppression of *LATS2* (which otherwise would permit the up-regulation of macrophage markers and inflammatory cytokines). Future studies are needed to fully investigate the CHI3L1-LATS2 axis in atherosclerosis.

Taken together, this study suggests that CHI3L1 may play a key role in vascular pathology and should be investigated as a new translational target for CVD. Using two large, independent human biobanks, we confirm that CHI3L1 is a powerful mediator of carotid disease. These findings support other reports[43] suggesting that CHI3L1 has the capacity to differentiate which subjects are at highest risk for a future clinical event. Mechanistically, we report that CHI3L1 prevents maladaptive changes in vascular SMCs, preserving a phenotype that appears to stabilize the vulnerable atherosclerotic plaque. This effect seems to occur as a compensatory response to the complex pro-atherogenic milieu of the plaque and may be mediated via the downstream suppression of the tumour suppressor gene, *LATS2*. While future studies are needed to understand the context-dependent properties of this key acute phase reactant, understanding how to measure and modulate CHI3L1 could have a role in the diagnosis and management of patients with cerebrovascular disease at risk for stroke.

Supplementary material

Supplementary material is available at *Cardiovascular Research* online.

Authors' contributions

L.M. and N.J.L. conceived the study. P.T. and S.L. designed and conducted the majority of experiments. Z.W. and V.P. performed immunohistochemistry and immunofluorescent stainings and parts of the *in vitro* experiments. A.E. and M.V. performed parts of the *in vitro* experiments. V.P., G.W., and S.L. performed the RNAseq analysis. J.Y. and K.-U.J. assisted in performing the mouse surgeries. J.P. conducted human plaque processing of the MVB. L.M. and U.H. conducted the human plaque processing of BiKE and performed mRNA expression analysis and protein quantification. V.N., Y.W., Y.K. and A.F., H.-H.E., and P.S.T. contributed to experimental design and data interpretation. L.M., N.L., P.T., and S.L. wrote the manuscript. Results were discussed and feedback to the manuscript was provided by all authors.

Conflict of interest: none declared.

Data availability

The data underlying this article are available in the article and in its online Supplementary material.

References

1. World Health Organisation - Healthinfo on Global Burden Disease. https://www.who.int/healthinfo/global_burden_disease/GHE2016_Deaths_Global_2000_2016.xls (6 February 2020, date last accessed).
2. Lozano R, Naghavi M, Foreman K, Lim S, Shibuya K, Aboyans V, Abraham J, Adair T, Aggarwal R, Ahn SY, Alvarado M, Anderson HR, Anderson LM, Andrews KG, Atkinson C, Baddour LM, Barker-Collo S, Bartels DH, Bell ML, Benjamin EJ, Bennett D, Bhalla K, Bikbov B, Bin Abdulhak A, Birbeck G, Blyth F, Bolliger I, Boufous S, Bucello C, Burch M, Burney P, Carapetis J, Chen H, Chou D, Chugh SS, Coffeng LE, Colan SD, Colquhoun S, Colson KE, Condon J, Connor MD, Cooper LT, Corriere M, Cortinovis M, de Vaccaro KC, Couser W, Cowie BC, Criqui MH, Cross M, Dabhadkar KC, Dahodwala N, De Leo D, Degenhardt L, Delossantos A, Denenberg J, Des Jarlais DC, Dharmaratne SD, Dorsey ER, Driscoll T, Duber H, Ebel B, Erwin PJ, Espindola P, Ezzati M, Feigin V, Flaxman AD, Forouzanfar MH, Fowkes FG, Franklin R, Fransen M, Freeman MK, Gabriel SE, Gakidou E, Gaspari F, Gillum RF, Gonzalez-Medina D, Halasa YA, Haring D, Harrison JE, Havmoeller R, Hay RJ, Hoen B, Hotez PJ, Hoy D, Jacobsen KH, James SL, Jasrasaria R, Jayaraman S, Johns N, Karthikeyan G, Kassebaum N, Keren A, Khoo JP, Knowlton LM, Kobusingye O, Koranteng A, Krishnamurthi R, Lipnick M, Lipshultz SE, Ohno SL, Mabweijano J, MacIntyre MF, Mallinger L, March L, Marks GB, Marks R, Matsumori A, Matzopoulos R, Mayosi BM, McAnulty JH, McDermott MM, McGrath J, Mensah GA, Merriman TR, Michaud C, Miller M, Miller TR, Mock C, Mocumbi AO, Mokdad AA, Moran A, Mulholland K, Nair MN, Naldi L, Narayan KM, Nasseri K, Norman P, O'Donnell M, Omer SB, Ortblad K, Osborne R, Ozgediz D, Pahari B, Pandian JD, Rivero AP, Padilla RP, Perez-Ruiz F, Perico N, Phillips D, Pierce K, Pope CA III, Porrini E, Pourmalek F, Raju M, Ranganathan D, Rehm JT, Rein DB, Remuzzi G, Rivara FP, Roberts T, De Leon FR, Rosenfeld LC, Rushton L, Sacco RL, Salomon JA, Sampson U, Sanman E, Schwebel DC, Segui-Gomez M, Shepard DS, Singh D, Singleton J, Sliwa K, Smith E, Steer A, Taylor JA, Thomas B, Tleyjeh IM, Towbin JA, Truelsen T, Undurraga EA, Venketasubramanian N, Vijayakumar L, Vos T, Wagner GR, Wang M, Wang W, Watt K, Weinstock MA, Weintraub R, Wilkinson JD, Woolf AD, Wulf S, Yeh PH, Yip P, Zabetian A, Zheng ZJ, Lopez AD, Murray CJ, AlMazroa MA, Memish ZA. Global and regional mortality from 235 causes of death for 20 age groups in 1990 and 2010: a systematic analysis for the global burden of disease study 2010. *Lancet* 2012;**380**:2095–2128.
3. Furie KL, Kasner SE, Adams RJ, Albers GW, Bush RL, Fagan SC, Halperin JL, Johnston SC, Katzan I, Kernan WN, Mitchell PH, Ovbiagele B, Palesch YY, Sacco RL, Schwamm LH, Wassertheil-Smoller S, Turan TN, Wentworth D, American Heart Association Stroke Council CoCNCoCC, Interdisciplinary Council on Quality of C, Outcomes R. Guidelines for the prevention of stroke in patients with stroke or transient ischemic attack: a guideline for healthcare professionals from the American Heart Association/American Stroke Association. *Stroke* 2011;**42**:227–276.
4. Libby P, Ridker PM, Hansson GK. Progress and challenges in translating the biology of atherosclerosis. *Nature* 2011;**473**:317–325.
5. Naylor AR, Ricco JB, de Borst GJ, Debus S, de Haro J, Halliday A, Hamilton G, Kakisis J, Kakkos S, Lepidi S, Markus HS, McCabe DJ, Roy J, Sillesen H, van den Berg JC, Vermassen F, Esvs Guidelines C, Kolh P, Chakfe N, Hinchliffe RJ, Koncar I, Lindholt JS, Vega de Ceniga M, Verzini F, Esvs Guideline R, Archie J, Bellmunt S, Chaudhuri A, Koelemay M, Lindahl AK, Padberg F, Venermo M. Editor's choice - management of atherosclerotic carotid and vertebral artery disease: 2017 clinical practice guidelines of the European Society for Vascular Surgery (ESVS). *Eur J Vasc Endovasc Surg* 2018;**55**:3–81.
6. Maegdefessel L. The emerging role of microRNAs in cardiovascular disease. *J Intern Med* 2014;**276**:633–644.
7. Hgnc Website, Chi3l1 Symbol Report. https://www.genenames.org/data/gene-symbol-report/#!/hgnc_id/HGNC:1932 (1 September 2020, date last accessed).
8. Lee CG, Da Silva CA, Dela Cruz CS, Ahangari F, Ma B, Kang MJ, He CH, Takyar S, Elias JA. Role of chitin and chitinase/chitinase-like proteins in inflammation, tissue remodeling, and injury. *Annu Rev Physiol* 2011;**73**:479–501.
9. Perisic L, Aldi S, Sun Y, Folkersen L, Razuvaev A, Roy J, Lengquist M, Akesson S, Wheelock CE, Maegdefessel L, Gabrielsen A, Odeberg J, Hansson GK, Paulsson-Berne G, Hedin U. Gene expression signatures, pathways and networks in carotid atherosclerosis. *J Intern Med* 2016;**279**:293–308.
10. Bara I, Ozier A, Girodet PO, Carvalho G, Cattiaux J, Begueret H, Thumerel M, Ousova O, Kolbeck R, Coyle AJ, Woods J, Tunon de Lara JM, Marthan R, Berger P. Role of Ykl-40 in bronchial smooth muscle remodeling in asthma. *Am J Respir Crit Care Med* 2012;**185**:715–722.
11. Harutyunyan M, Christiansen M, Johansen JS, Kober L, Torp-Petersen C, Kastrup J. The inflammatory biomarker Ykl-40 as a new prognostic marker for all-cause mortality in patients with heart failure. *Immunobiology* 2012;**217**:652–656.
12. Kastrup J. Can Ykl-40 be a new inflammatory biomarker in cardiovascular disease? *Immunobiology* 2012;**217**:483–491.
13. Marott SCW, Benn M, Johansen JS, Jensen GB, Tybjærg-Hansen A, Nordestgaard BG. Ykl-40 levels and atrial fibrillation in the general population. *Int J Cardiol* 2013;**167**:1354–1359.
14. Nojgaard C, Host NB, Christensen IJ, Poulsen SH, Egstrup K, Price PA, Johansen JS. Serum levels of Ykl-40 increases in patients with acute myocardial infarction. *Coron Artery Dis* 2008;**19**:257–263.
15. Vos K, Steenbakkers P, Miltenburg AM, Bos E, van Den Heuvel MW, van Hogezand RA, de Vries RR, Breedveld FC, Boots AM. Raised human cartilage glycoprotein-39 plasma levels in patients with rheumatoid arthritis and other inflammatory conditions. *Ann Rheum Dis* 2000;**59**:544–548.
16. Wang Y, Ripa RS, Johansen JS, Gabrielsen A, Steinbrüchel DA, Friis T, Bindslev L, Haack-Sørensen M, Jørgensen E, Kastrup J. Ykl-40 a new biomarker in patients with acute coronary syndrome or stable coronary artery disease. *Scand Cardiovasc J* 2008;**42**:295–302.
17. Lin CH, Li HY, Jiang YD, Chang TJ, Chuang LM. Plasma Ykl-40 predicts 10-year cardiovascular and all-cause mortality in individuals with type 2 diabetes. *Clin Endocrinol* 2013;**79**:185–191.
18. Johansen JS, Bojesen SE, Tybjærg-Hansen A, Mylin AK, Price PA, Nordestgaard BG. Plasma Ykl-40 and total and disease-specific mortality in the general population. *Clin Chem* 2010;**56**:1580–1591.
19. Kornblit B, Hellemann D, Munthe-Fog L, Bonde J, Strom JJ, Madsen HO, Johansen JS, Garred P. Plasma Ykl-40 and Chi3l1 in systemic inflammation and sepsis-experience from two prospective cohorts. *Immunobiology* 2013;**218**:1227–1234.
20. Mygind ND, Iversen K, Kober L, Goetze JP, Nielsen H, Boesgaard S, Bay M, Johansen JS, Nielsen OW, Kirk V, Kastrup J. The inflammatory biomarker Ykl-40 at admission is a strong predictor of overall mortality. *J Intern Med* 2013;**273**:205–216.
21. Konradsen JR, James A, Nordlund B, Reinius LE, Soderhall C, Melen E, Wheelock AM, Lodrup Carlsen KC, Lidegran M, Verhoek M, Boot RG, Dahlen B, Dahlen SE, Hedlin G. The chitinase-like protein Ykl-40: a possible biomarker of inflammation and airway remodeling in severe pediatric asthma. *J Allergy Clin Immunol* 2013;**132**:328–335.E5.
22. Matsumoto T, Tsurumoto T. Serum Ykl-40 levels in rheumatoid arthritis: correlations between clinical and laborarory parameters. *Clin Exp Rheumatol* 2001;**19**:655–660.
23. Maegdefessel L, Spin JM, Raaz U, Eken SM, Toh R, Azuma J, Adam M, Nagakami F, Heymann HM, Chernugobova E, Jin H, Roy J, Hultgren R, Caidahl K, Schrepfer S, Hamsten A, Eriksson P, McConnell MV, Dalman RL, Tsao PS. 24 limits aortic vascular inflammation and murine abdominal aneurysm development. *Nat Commun* 2014;**5**:5214.
24. Michelsen AE, Rathcke CN, Skjelland M, Holm S, Ranheim T, Krohg-Sorensen K, Klingvall MF, Brosstad F, Oie E, Vestergaard H, Aukrust P, Halvorsen B. Increased Ykl-40 expression in patients with carotid atherosclerosis. *Atherosclerosis* 2010;**211**:589–595.
25. Jung YY, Kim KC, Park MH, Seo Y, Park H, Park MH, Chang J, Hwang DY, Han SB, Kim S, Son DJ, Hong JT. Atherosclerosis is exacerbated by chitinase-3-like-1 in amyloid precursor protein transgenic mice. *Theranostics* 2018;**8**:749–766.
26. Gong Z, Xing S, Zheng F, Xing Q. Increased expression of chitinase 3-like 1 in aorta of patients with atherosclerosis and suppression of atherosclerosis in apolipoprotein E-knockout mice by chitinase 3-like 1 gene silencing. *Mediators Inflamm* 2014;**2014**:1–12.
27. Zhang H, Zhou W, Cao C, Zhang W, Liu G, Zhang J. Amelioration of atherosclerosis in apolipoprotein E-deficient mice by combined RNA interference of lipoprotein-associated phospholipase A2 and Ykl-40. *PLoS One* 2018;**13**:e0202797.
28. Gorgens SW, Hjorth M, Eckardt K, Wichert S, Norheim F, Holen T, Lee S, Langleite T, Birkeland KI, Stadheim HK, Kolnes KJ, Tangen DS, Kolnes AJ, Jensen J, Drevon CA, Eckel J. The exercise-regulated myokine chitinase-3-like protein 1 stimulates human myocyte proliferation. *Acta Physiol (Oxf)* 2016;**216**:330–345.
29. Nishikawa KC, Millis AJT. Gp38k (Chi3l1) is a novel adhesion and migration factor for vascular cells. *Exp Cell Res* 2003;**287**:79–87.
30. Matic LP, Jesus Iglesias M, Vesterlund M, Lengquist M, Hong M-G, Saieed S, Sanchez-Rivera L, Berg M, Razuvaev A, Kronqvist M, Lund K, Caidahl K, Gillgren P, Pontén F, Uhlén M, Schwenk JM, Hansson GK, Paulsson-Berne G, Fagman E, Roy J, Hultgren R, Bergström G, Lehtiö J, Odeberg J, Hedin U. Novel multiomics profiling of human carotid atherosclerotic plaques and plasma reveals biliverdin reductase B as a marker of intraplaque hemorrhage. *JACC Basic Transl Sci* 2018;**3**:464–480.

31. Branca RMM, Orre LM, Johansson HJ, Granholm V, Huss M, Pérez-Bercoff Å, Forshed J, Käll L, Lehtiö J. Hirief Lc-Ms enables deep proteome coverage and unbiased proteogenomics. *Nat Methods* 2014;**11**:59–62.

32. Anderson JD, Johansson HJ, Graham CS, Vesterlund M, Pham MT, Bramlett CS, Montgomery EN, Mellema MS, Bardini RL, Contreras Z, Hoon M, Bauer G, Fink KD, Fury B, Hendrix KJ, Chedin F, EL-Andaloussi S, Hwang B, Mulligan MS, Lehtiö J, Nolta JA. Comprehensive proteomic analysis of mesenchymal stem cell exosomes reveals modulation of angiogenesis via nuclear factor-kappaB signaling. *Stem Cells* 2016;**34**: 601–613.

33. Jin H, Li DY, Chernogubova E, Sun C, Busch A, Eken SM, Saliba-Gustafsson P, Winter H, Winski G, Raaz U, Schellinger IN, Simon N, Hegenloh R, Matic LP, Jagodic M, Ehrenborg E, Pelisek J, Eckstein HH, Hedin U, Backlund A, Maegdefessel L. Local delivery of Mir-21 stabilizes fibrous caps in vulnerable atherosclerotic lesions. *Mol Ther* 2018;**26**:1040–1055.

34. Pelisek J, Hegenloh R, Bauer S, Metschl S, Pauli J, Glukha N, Busch A, Reutersberg B, Kallmayer M, Trenner M, Wendorff H, Tsantilas P, Schmid S, Knappich C, Schaeffer C, Stadlbauer T, Biro G, Wertern U, Meisner F, Stoklasa K, Menges AL, Radu O, Dallmann-Sieber S, Karlas A, Knipfer E, Reeps C, Zimmermann A, Maegdefessel L, Eckstein HH. Biobanking: objectives, requirements, and future challenges-experiences from the Munich Vascular Biobank. *JCM* 2019;**8**:251.

35. Redgrave JN, Gallagher P, Lovett JK, Rothwell PM. Critical cap thickness and rupture in symptomatic carotid plaques: the Oxford plaque study. *Stroke* 2008;**39**:1722–1729.

36. Eken SM, Jin H, Chernogubova E, Li Y, Simon N, Sun C, Korzunowicz G, Busch A, Backlund A, Osterholm C, Razuvaev A, Renne T, Eckstein HH, Pelisek J, Eriksson P, Gonzalez Diez M ,P, Matic, L Schellinger, IN Raaz, U Leeper, NJ Hansson, GK Paulsson-Berne, G Hedin, U Maegdefessel, L. Microrna-210 enhances fibrous cap stability in advanced atherosclerotic lesions. *Circ Res* 2017;**120**:633–644.

37. Khatri P, Sirota M, Butte AJ. Ten years of pathway analysis: current approaches and outstanding challenges. *PLoS Comput Biol* 2012;**8**:e1002375.

38. Leeper NJ, Raiesdana A, Kojima Y, Kundu RK, Cheng H, Maegdefessel L, Toh R, Ahn GO, Ali ZA, Anderson DR, Miller CL, Roberts SC, Spin JM, de Almeida PE, Wu JC, Xu B, Cheng K, Quertermous M, Kundu S, Kortekaas KE, Berzin E, Downing KP, Dalman RL, Tsao PS, Schadt EE, Owens GK, Quertermous T. Loss of Cdkn2b promotes P53-dependent smooth muscle cell apoptosis and aneurysm formation. *Arterioscler Thromb Vasc Biol* 2013;**33**:e1–e10.

39. Sasaki T, Kuzuya M, Nakamura K, Cheng XW, Shibata T, Sato K, Iguchi A. A simple method of plaque rupture induction in apolipoprotein E-deficient mice. *Arterioscler Thromb Vasc Biol* 2006;**26**:1304–1309.

40. Hartwig H, Silvestre-Roig C, Hendrikse J, Beckers L, Paulin N, Van der Heiden K, Braster Q, Drechsler M, Daemen MJ, Lutgens E, Soehnlein O. Atherosclerotic plaque destabilization in mice: a comparative study. *PLoS One* 2015;**10**:e0141019.

41. Kastrup J, Johansen JS, Winkel P, Hansen JF, Hildebrandt P, Jensen GB, Jespersen CM, Kjoller E, Kolmos HJ, Lind I, Nielsen H, Gluud C, Group CT, the CLARICOR Trial Group. High serum Ykl-40 concentration is associated with cardiovascular and all-cause mortality in patients with stable coronary artery disease. *Eur Heart J* 2009;**30**: 1066–1072.

42. Ridker PM, Chasman DI, Rose L, Loscalzo J, Elias JA. Plasma levels of the proinflammatory chitin-binding glycoprotein Ykl-40, variation in the chitinase 3-like 1 gene (Chi3l1), and incident cardiovascular events. *J Am Heart Assoc* 2014;**3**:e000897.

43. Langley SR, Willeit K, Didangelos A, Matic LP, Skroblin P, Barallobre-Barreiro J, Lengquist M, Rungger G, Kapustin A, Kedenko L, Molenaar C, Lu R, Barwari T, Suna G, Yin X, Iglseder B, Paulweber B, Willeit P, Shalhoub J, Pasterkamp G, Davies AH, Monaco C, Hedin U, Shanahan CM, Willeit J, Kiechl S, Mayr M. Extracellular matrix proteomics identifies molecular signature of symptomatic carotid plaques. *J Clin Invest* 2017;**127**:1546–1560.

44. Park HY, Jun CD, Jeon SJ, Choi SS, Kim HR, Choi DB, Kwak S, Lee HS, Cheong JS, So HS, Lee YJ, Park DS. Serum Ykl-40 levels correlate with infarct volume, stroke severity, and functional outcome in acute ischemic stroke patients. *PLoS One* 2012;**7**: e51722.

45. Kjaergaard AD, Bojesen SE, Johansen JS, Nordestgaard BG. Elevated plasma Ykl-40 levels and ischemic stroke in the general population. *Ann Neurol* 2010;**68**:672–680.

46. Kjaergaard AD, Johansen JS, Bojesen SE, Nordestgaard BG. Elevated plasma Ykl-40, lipids and lipoproteins, and ischemic vascular disease in the general population. *Stroke* 2015;**46**:329–335.

47. Kzhyshkowska J, Gratchev A, Goerdt S. Human chitinases and chitinase-like proteins as indicators for inflammation and cancer. *Biomark Insights* 2007;**2**:128–146.

48. Boot RG, van Achterberg TA, van Aken BE, Renkema GH, Jacobs MJ, Aerts JM, de Vries CJ. Strong induction of members of the chitinase family of proteins in atherosclerosis: chitotriosidase and human cartilage Gp-39 expressed in lesion macrophages. *Arterioscler Thromb Vasc Biol* 1999;**19**:687–694.

49. Jung TW, Park HS, Choi GH, Kim D, Jeong JH, Lee T. Chitinase-3-like protein 1 ameliorates atherosclerotic responses via PPARdelta-mediated suppression of inflammation and ER stress. *J Cell Biochem* 2018;**119**:6795–6805.

50. Gorgens SW, Eckardt K, Elsen M, Tennagels N, Eckel J. Chitinase-3-like protein 1 protects skeletal muscle from TNFalpha-induced inflammation and insulin resistance. *Biochem J* 2014;**459**:479–488.

51. Ling H, Recklies AD. The chitinase 3-like protein human cartilage glycoprotein 39 inhibits cellular responses to the inflammatory cytokines interleukin-1 and tumour necrosis factor-alpha. *Biochem J* 2004;**380**:651–659.

52. Furth N, Aylon Y. The lats1 and lats2 tumor suppressors: beyond the hippo pathway. *Cell Death Differ* 2017;**24**:1488–1501.

Translational perspective

Taken together, CHI3L1 has the potential to become a new translational target for cardiovascular disease. With further studies to understand its full causal relationship to inflammatory pathways, it could have a role in the diagnosis and management of patients with cerebrovascular disease at risk for stroke.